Supporting Information

High-performance sodium-ion anodes enabled by a low-temperature molten salt approach

Lei Liu[#], Jinmeng Sun[#], Zhuzhu Du,* Ke Wang, Yuhang Liu, Song He, Hongfang Du, Wei Ai* and Wei Huang*

1. Experimental section

1.1 Synthesis of NS-FLG materials

GO was prepared by a modified Hummers' method. For the preparation of NS-FLG, 1 g GO was dispersed in 100 mL deionized water by ultrasonication for 30 min to obtain a brownish-yellow dispersion. Subsequently, a solution containing 40 g KSCN dissolved in 40 mL deionized water was dropwise added to the above GO dispersion. The mixed solution was stirred at room temperature for 30 min and then dried at 100 ℃ to obtain GO@KSCN composite. Afterward, the composite was annealed under argon atmosphere with a heating rate of 5 ℃ min^{-1} to the purposed temperature (150, 175, and 300 °C) for 12 h. Finally, the product was washed with deionized water for several times, and dried at 100 ℃ overnight.

### 1.2 Materials characterization

Scanning electron microscopy and Transmission electron microscopy were acquired on a Verios G4 and FEI Talos F200X TEM, respectively. X-ray powder diffraction patterns were measured on a Bruker D8 advance diffractometer with Cu Kα radiation. X-ray photoelectron spectroscopy was tested using an Axis Supra XPS spectrometer equipped with monochromated Al Kα. Raman spectroscopy was collected using a Horiba LabRAM Evolution spectrometer with an excitation wavelength of 532 nm. N$_2$ adsorption-desorption analysis was obtained on an ASAP2460 apparatus.

### 1.3 Electrochemical characterization

The electrode was prepared by mixing 80 wt% of active materials, 10 wt% of acetylene black, and 10 wt% of polyvinylidene fluoride in N-methyl-2-pyrrolidone,

after which the slurry was coated onto a copper foil and dried overnight at 80 °C under vacuum. The cells were assembled using NS-FLG as the working electrode, Na metal sheet as the counter electrode, and 1 M $NaPF_6$ in dimethyl ether as the electrolyte. Electrochemical tests were performed in the voltage range of 0.01-3.0 V (vs. Na/Na$^+$) using a NEWARE battery testing system and a CHI 760D electrochemical workstation.
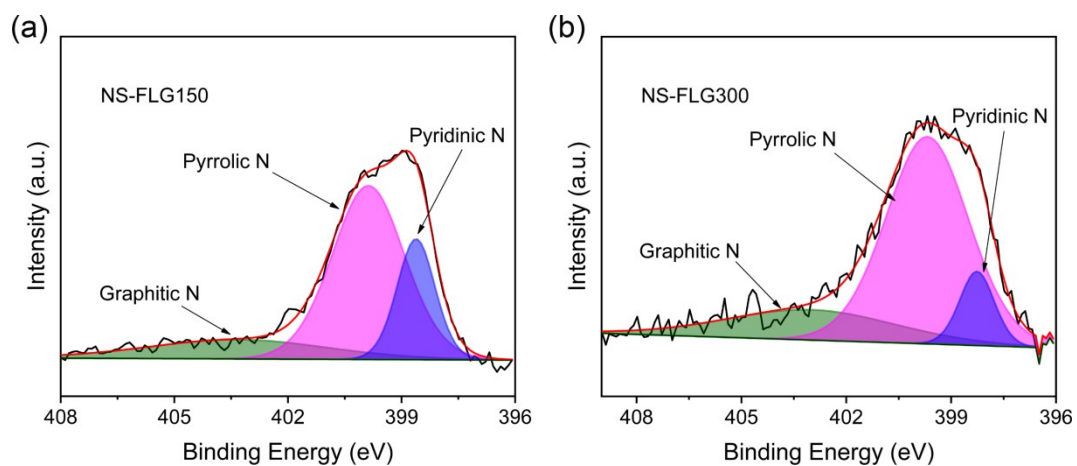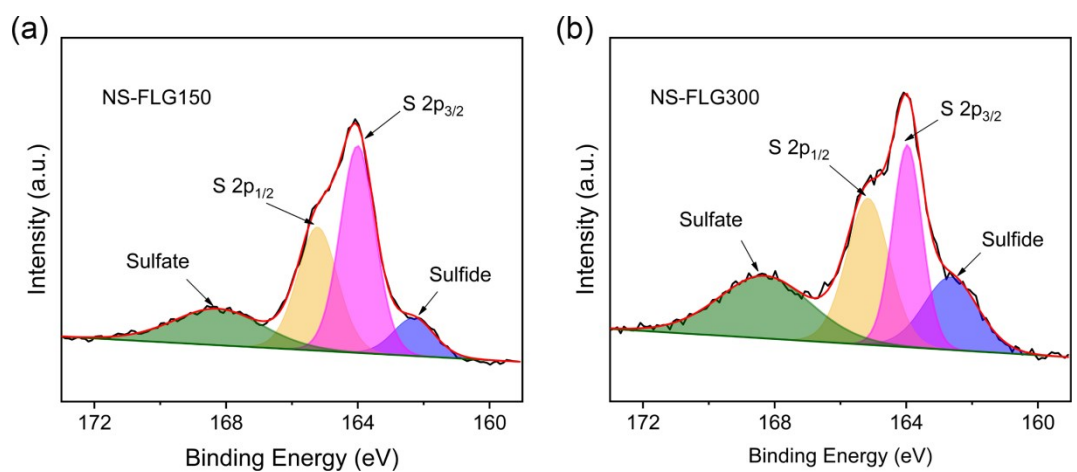
2. Supplementary figures
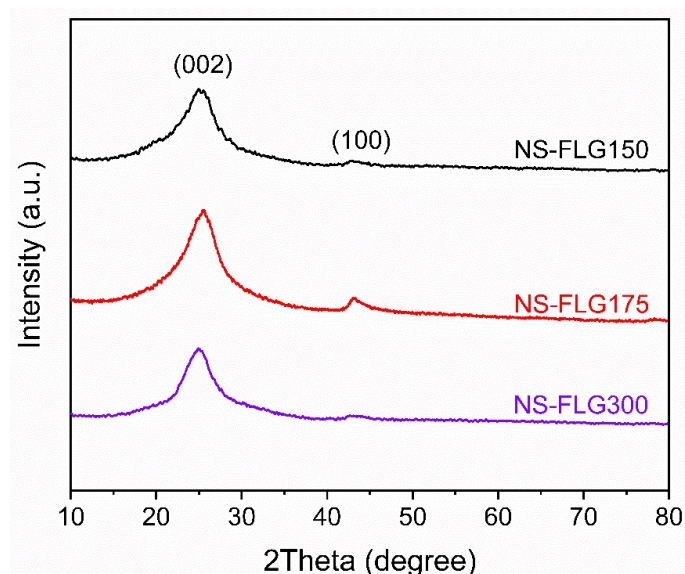
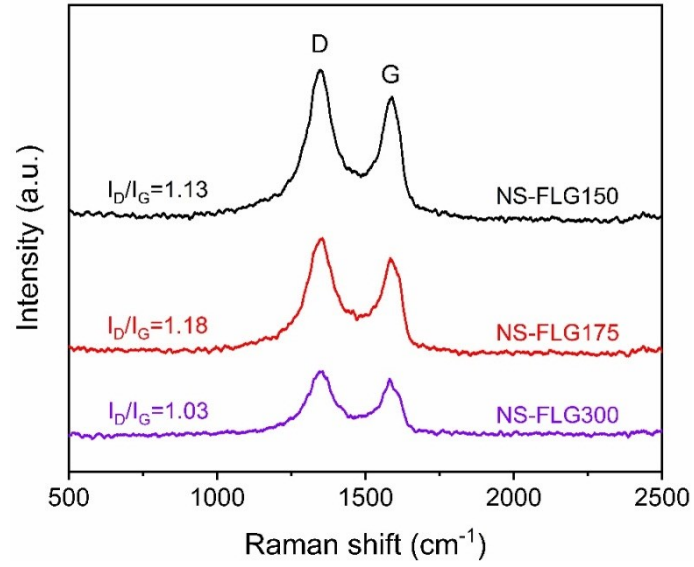**Fig. S1** XRD patterns of NS-FLG150, NS-FLG175, and NS-FLG300.
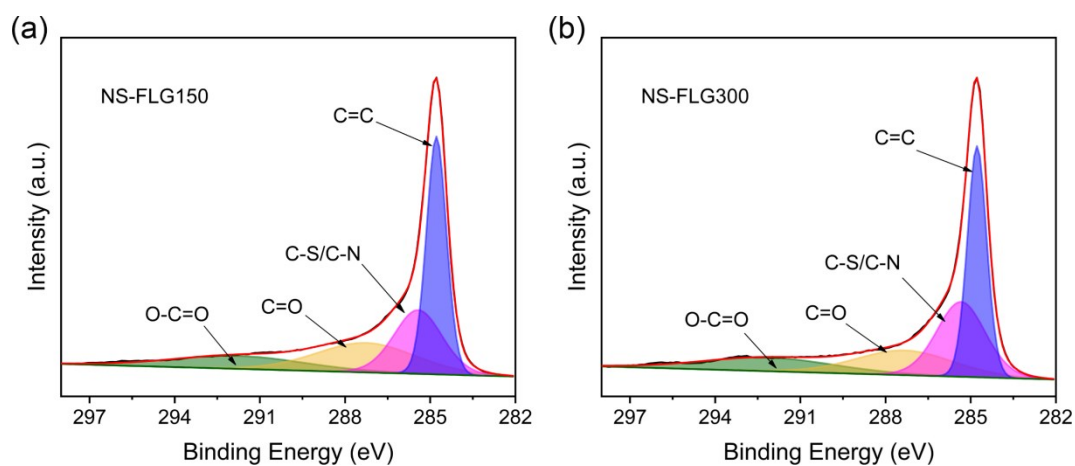
Fig. S2 High-resolution C 1s XPS spectra of (a) NS-FLG150 and (b) NS-FLG300.
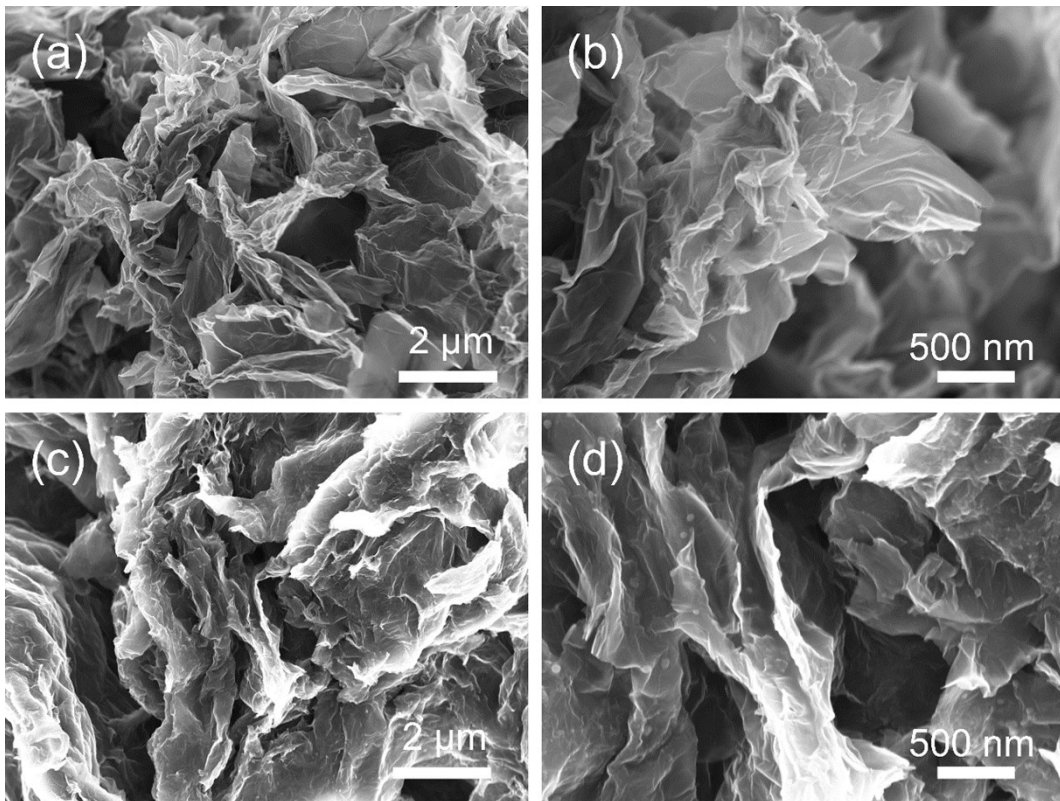
Fig. S3 High-resolution N 1s XPS spectra of (a) NS-FLG150 and (b) NS-FLG300.
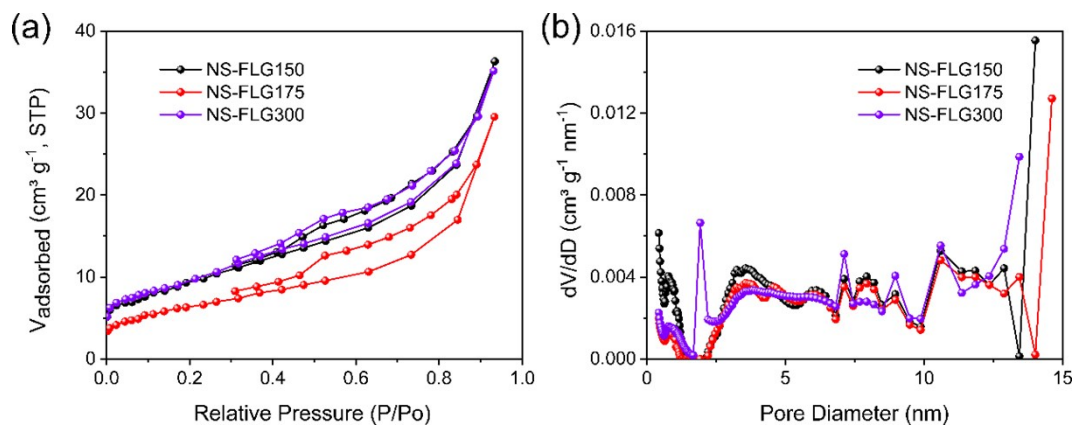

Fig. S4 High-resolution S 2p XPS spectra of (a) NS-FLG150 and (b) NS-FLG300.

Fig. S5 Raman spectra of NS-FLG150, NS-FLG175, and NS-FLG300.

Fig. S6 SEM images of (a-b) NS-FLG150 and (c-d) NS-FLG300.

Fig. S7 (a) N$_2$ adsorption-desorption isotherms and (b) the corresponding NLDFT pore size distribution plots of NS-FLG150, NS-FLG175, and NS-FLG300.
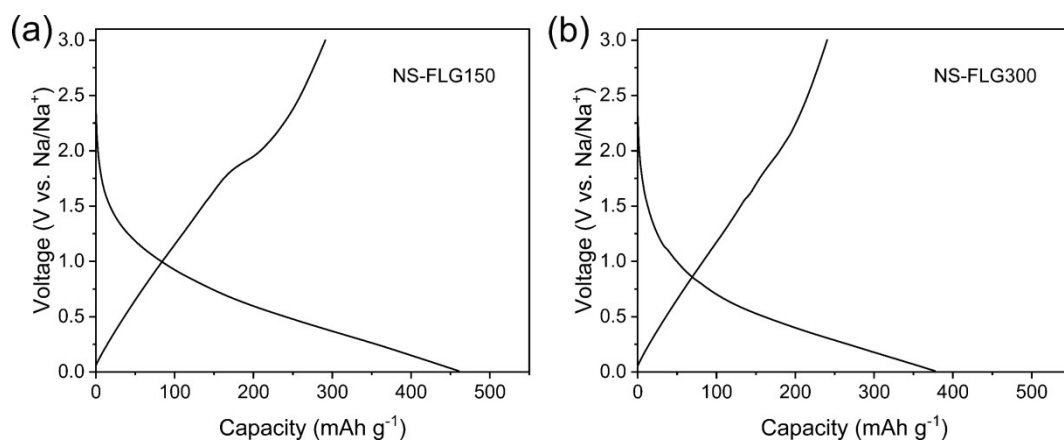
Fig. S8 The initial galvanostatic charge/discharge profiles of (a) NS-FLG150 and (b) NS-FLG300 at a current density of 0.5 A g^{-1}.
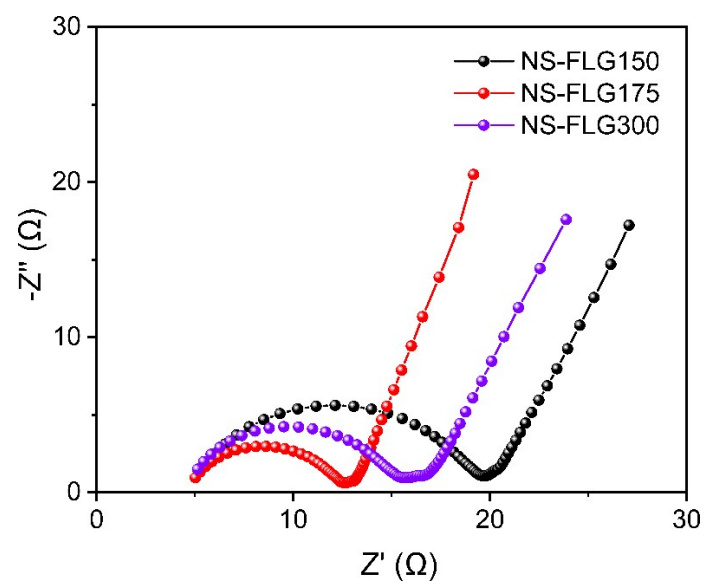
Fig. S9 Nyquist plots of the NS-FLG150, NS-FLG175, and NS-FLG300 electrodes.

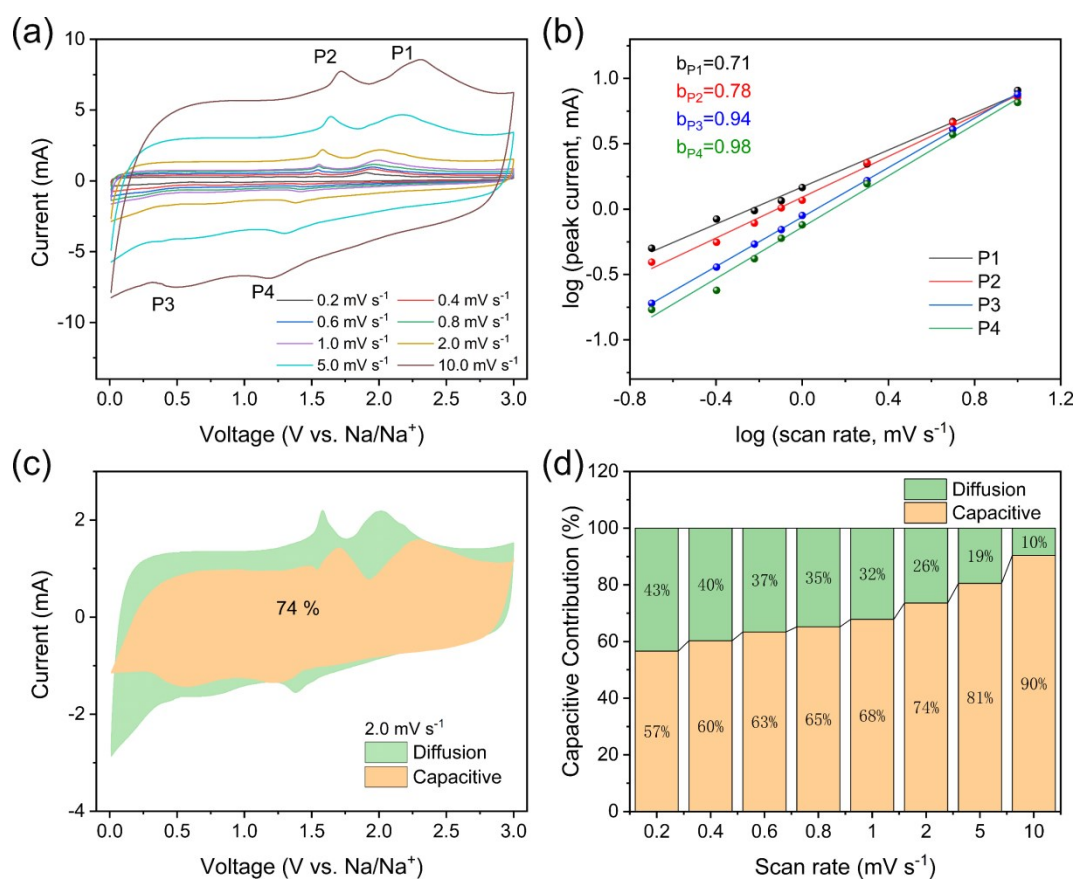**Fig. S10** (a) CV curves of NS-FLG150 anode at different scan rates ranging from 0.2 to 10.0 mV s^{-1}. (b) Linear relationships between log i and log v profiles, where i and v represent peak current and scan rate, respectively. (c) Capacitive and diffusion-controlled contributions to the Na$^+$ storage in NS-FLG150 at 2.0 mV s^{-1}. (d) Normalized contributions of capacitive and diffusion-controlled processes to the total capacity of NS-FLG150 at various scan rates.
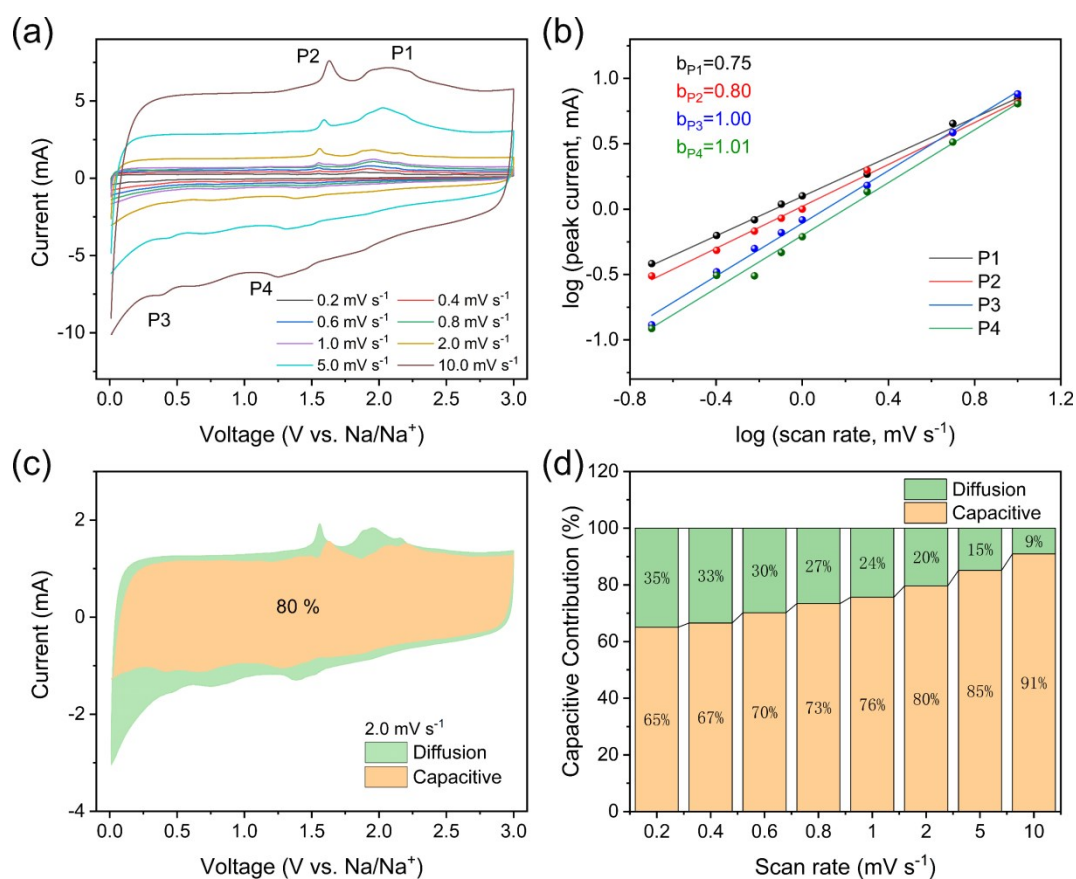
Fig. S11 (a) CV curves of NS-FLG300 anode at different scan rates ranging from 0.2 to 10.0 mV s^{-1}. (b) Linear relationships between log i and log v profiles, where i and v represent peak current and scan rate, respectively. (c) Capacitive and diffusion-controlled contributions to the Na$^+$ storage in NS-FLG300 at 2.0 mV s^{-1}. (d) Normalized contributions of capacitive and diffusion-controlled processes to the total capacity of NS-FLG300 at various scan rates.

3. Supplementary tables

Table S1. XPS results of NS-FLG150, NS-FLG175, and NS-FLG300.

Samples	XPS (at %)			
	C	N	S	O
NS-FLG150	85.64	2.34	2.02	10.0
NS-FLG175	84.72	3.53	2.90	8.85
NS-FLG300	92.84	2.35	1.49	3.32

Table S2. Nitrogen content and percentage of different nitrogen species for NS-FLG150, NS-FLG175, and NS-FLG300.

Sample	Total N (at%)	Quaternary N (at%)	Pyrrolic N (at%)	Pyridinic N (at%)	Quaternary N (%)	Pyrrolic N (%)	Pyridinic N (%)
NS-FLG150	2.34	0.39	1.43	0.52	16.67	61.11	22.22
NS-FLG175	3.53	1.49	1.02	1.02	42.20	28.90	28.90
NS-FLG300	2.35	0.49	1.62	0.24	20.85	68.94	10.21

Table S3. BET analysis of NS-FLG150, NS-FLG175, and NS-FLG300.

Samples	Monolayer adsorption Volume (cm^3 STP g^{-1})	BET surface area (m^2 g^{-1})	Total pore volume (cm^3 g^{-1})	Mean pore diameter (nm)
NS-FLG150	7.86	34.21	0.056	6.56
NS-FLG175	6.55	28.25	0.050	7.07
NS-FLG300	7.93	34.52	0.054	6.30

Table S4. Comparison of our NS-FLG175 with the previously reported carbon-based anodes in SIBs.

Samples	Voltage window (V vs. Na/Na$^+$)	Rate capacity	Cyclic stability	Initial coulombic efficiency (%)	Ref
N and S co-doped graphene nanosheets	0.01 - 3.0	141 mAh g^{-1} at 5.0 A g^{-1}	260 mAh g^{-1} at 1.0 A g^{-1} (10000 cycles)	50.86	1
N and S co-doped graphene nanosheets	0.01 - 3.0	144 mAh g^{-1} at 10 A g^{-1}	153 mAh g^{-1} at 5.0 A g^{-1} (5000 cycles)	52	2
N and F co-doped graphene paper	0.01 - 3.0	50 mAh g^{-1} at 1.0 A g^{-1}	56.3 mAh g^{-1} at 1.0 A g^{-1} (5000 cycles)	40.7	3
N and S co-doped mesoporous carbon nanofiber	0.1 - 3.0	121.8 mAh g^{-1} at 10.0 A g^{-1}	160.2 mAh g^{-1} at 10.0 A g^{-1} (10000 cycles)	—	4
N and S co-doped hierarchically porous carbon	0.01 - 2.50	176 mAh g^{-1} at 2.0 A g^{-1}	248 mAh g^{-1} at 0.1 A g^{-1} (500 cycles)	34.4	5
N and S co-doped carbon	0.01 - 3.0	131 mAh g^{-1} at 5.0 A g^{-1}	150 mAh g^{-1} at 0.5 A g^{-1} (3400 cycles)	—	6
N and S co-doped carbon films	0.01 - 3.0	92.2 mAh g^{-1} at 2.0 A g^{-1}	379.1 mAh g^{-1} at 0.1 A g^{-1} (1000 cycles)	—	7
N and S co-doped hollow carbon spheres	0.01 - 3.0	110 mAh g^{-1} at 10 A g^{-1}	169 mAh g^{-1} at 0.5 A g^{-1} (2000 cycles)	—	8
N and O co-doped holey graphene	0.01 - 3.0	189 mAh g^{-1} at 10.0 A g^{-1}	179 mAh g^{-1} at 5.0 A g^{-1} (2000 cycles)	44.1	9
P and S co-doped carbon	0.01 - 3.0	181.8 mAh g^{-1} at 10 A g^{-1}	290.1 mAh g^{-1} at 1.0 A g^{-1} (1000 cycles)	53.5	10
N doped carbon nanofibers	0.01 - 3.0	148 mAh g^{-1} at 10.0 A g^{-1}	146 mAh g^{-1} at 5.0 A g^{-1} (5000 cycles)	57	11
Holey graphene oxide	0.01 - 3.0	131 mAh g^{-1} at 10.0 A g^{-1}	163 mAh g^{-1} at 2.0 A g^{-1} (3000 cycles)	—	12
NS-FLG175	0.01 - 3.0	203 mAh g^{-1} at 10 A g^{-1}	243 mAh g^{-1} at 5.0 A g^{-1} (5100 cycles)	68.9	This work

References

1. Y. Ma, Q. Guo, M. Yang, Y. Wang, T. Chen, Q. Chen, X. Zhu, Q. Xia, S. Li and H. Xia, *Energy Storage Mater.*, 2018, **13**, 134.

2. X. Xu, H. Zeng, D. Han, K. Qiao, W. Xing, M. J. Rood and Z. Yan, *ACS Appl. Mater. Interfaces*, 2018, **10**, 37172.

3. H. An, Y. Li, Y. Gao, C. Cao, J. Han, Y. Feng and W. Feng, Carbon, 2017, **116**, 338.

4. M. Yu, Z. Yin, G. Yan, Z. Wang, H. Guo, G. Li, Y. Liu, L. Li and J. Wang, *J. Power Sources*, 2020, **449**, 227514.

5. X. Miao, D. Sun, X. Zhou and Z. Lei, *Chem. Eng. J.*, 2019, **364**, 208.

6. D. Xu, C. Chen, J. Xie, B. Zhang, L. Miao, J. Cai, Y. Huang and L. Zhang, *Adv. Energy Mater.*, 2016, **6**, 1501929.

7. J. Ruan, T. Yuan, Y. Pang, S. Luo, C. Peng, J. Yang and S. Zheng, *Carbon*, 2018, **126**, 9.

8. J. Ye, J. Zang, Z. Tian, M. Zheng and Q. Dong, *J. Mater. Chem. A*, 2016, **4**, 13223.

9. J. Zhao, Y. Zhang, J. Chen, W. Zhang, D. Yuan, R. Chua, H. N. Alshareef and Y. Ma, *Adv. Energy Mater.*, 2020, **10**, 2000099.

10. J. Yan, W. Li, P. Feng, R. Wang, M. Jiang, J. Han, S. Cao, K. Wang and K. Jiang, *J. Mater. Chem. A*, 2020, **8**, 422.

11. W. Zhao, X. Hu, S. Ci, J. Chen, G. Wang, Q. Xu and Z. Wen, *Small*, 2019, **15**, 1904054.

12. J. Zhao, Y. Z. Zhang, F. Zhang, H. F. Liang, F. W. Ming, H. N. Alshareef and Z. Q. Gao, *Adv. Energy Mater.*, 2019, **9**, 1803215.